

## Article

# Prediction of the Viscoelastic Properties of a Cetyl Pyridinium Chloride/Sodium Salicylate Micellar Solution: (II) Prediction of the Step Rate Experiments

Shuxin Huang <sup>1,2</sup> 

<sup>1</sup> Department of Engineering Mechanics, Shanghai Jiao Tong University, Shanghai 200240, China; huangshuxin@sjtu.edu.cn

<sup>2</sup> Key Laboratory of Hydrodynamics of the Ministry of Education, Shanghai Jiao Tong University, Shanghai 200240, China

**Abstract:** The reliable viscoelastic characterization and prediction of micellar solution is still required in industrial applications of the solution, e.g., in surfactant flooding and pharmaceuticals. Based on the recent theoretical characterization of the viscoelastic properties of a cetyl pyridinium chloride/sodium salicylate (CPyCl/NaSal) wormlike micellar solution with a structuralized constitutive model in the work published in 2022, the present work predicted five groups of transient shear viscoelasticities of the solution experimentally obtained in 2010, which include the first normal stress difference ( $N_1$ ) versus time curve in the start-up experiment, the shear stress ( $\tau_{12}$ ) in the start-up experiment,  $\tau_{12}$  in the long-term start-up experiment, the stress relaxation upon cessation of steady shear flow, and the transient  $N_1/\tau_{12}$  in the step strain experiment. The study findings clearly show an improvement in the predictions of the viscoelastic properties of the micellar solution compared with those predicted previously. For example, the experimental  $N_1/\tau_{12}$  is 9 at the strain of 9 in the step strain experiment, and the corresponding previous and present predictions are 2.47 and 8.45, respectively.

**Keywords:** micellar solution; viscoelastic property; constitutive equation; structuralized parameter; prediction



**Citation:** Huang, S. Prediction of the Viscoelastic Properties of a Cetyl Pyridinium Chloride/Sodium Salicylate Micellar Solution: (II) Prediction of the Step Rate Experiments. *Polymers* **2022**, *14*, 5561. <https://doi.org/10.3390/polym14245561>

Academic Editor: Peter Griffiths

Received: 25 November 2022

Accepted: 11 December 2022

Published: 19 December 2022

**Publisher's Note:** MDPI stays neutral with regard to jurisdictional claims in published maps and institutional affiliations.



**Copyright:** © 2022 by the author. Licensee MDPI, Basel, Switzerland. This article is an open access article distributed under the terms and conditions of the Creative Commons Attribution (CC BY) license (<https://creativecommons.org/licenses/by/4.0/>).

## 1. Introduction

Chemical flooding is an effective technology to enhance oil recovery [1,2] in the tertiary oil recovery process by increasing the viscosity of flooding fluid or reducing the interfacial tension between crude oil and reservoir brine. Surfactant flooding is a kind of chemical flooding [2–4] that can reduce the interfacial tension between oil and water and mobilize the trapped oil after water flooding. In recent decades, surfactant flooding has drawn increasing attention due to its merits, such as its interfacial property. Many studies have been conducted on both the physical properties of surfactant solution [1–6] and the numerical simulation of the flow of surfactant flooding [7,8]. A problem in these studies is that the present numerical simulation of surfactant flooding is not perfect, as the theoretical description of the flow property of surfactant solution still has defects. This hinders the theoretical analysis of surfactant flooding. Moreover, the theoretical viscoelastic analysis of micellar solution is also needed in other industries, e.g., cosmetic, food, and pharmaceutical.

The study status of the theoretical characterization of the viscoelastic property of micellar solution is introduced in the first part of the work of Huang [9] and indicates the deficiencies of the present theories. For example, the species-based Vasquez–Cook–McKinley model cannot describe the transient first normal stress difference of a micelle well [3], which is also shown in the present work. Also in the recent work [9], a modified Rivlin–Sawyers model was provided to characterize and predict the viscoelastic property of a micellar solution, which is based on the experimental viscoelasticity of the wormlike

micellar solution, i.e., 100 mM/50 mM of CPyCl/NaSal in a 100 mM NaCl solution, as obtained by Pipe et al. [3]. The shear viscoelastic characterization of the solution is provided in full in [9], which also shows the prediction of the steady shear experiment, indicating some successful aspect of the adopted model. Due to the limitation of the length of a paper, further predictions on the viscoelastic properties of the solution are not shown in [9].

A large number of the transient viscoelastic properties of the micellar solution are shown in the experimental work of Pipe et al. [3], which provides excellent viscoelastic data for checking the theoretical model. These are predicted in the present study using the proposed model and the viscoelastic characterization of the solution in [9]. The objective of the present work is to further examine the capability of the model in [9] based on the experiment in [3].

## 2. Materials and Methods

The viscoelastic experiment of the CPyCl/NaSal solution can be found in detail in the work of Pipe et al. [3], some of which was also introduced in the recent work of Huang [9]. Five groups of the transient viscoelastic experiments of the micelle are predicted here: the  $N_1$  versus time curve in the start-up experiment; the shear stress  $\tau_{12}$  in the start-up experiment; the shear stress in the long-term start-up experiment; the stress relaxation upon cessation of steady shear flow; and the transient  $N_1/\tau_{12}$  in the step strain experiment.

The modified Rivlin–Sawyers (RS) model [9] was used to characterize the viscoelastic property of the micellar solution, which stems from the recent works of Huang [10–12] and is written as:

$$\tau = \int_{-\infty}^t m(t-t', f, \zeta) \cdot h(\gamma) \cdot [\delta - C_t^{-1}(t')] dt' \quad (1)$$

where  $m(t-t', f, \zeta)$  is the time- and shear-rate-dependent memory function with the structure effect induced by shear rate;  $t$  and  $t'$  are the present and past time, respectively;  $f$  and  $\zeta$  are two scalar structuralized parameters, respectively;  $h$  is a strain-dependent function;  $\gamma$  is shear strain;  $\delta$  is a unit tensor; and  $C_t^{-1}$  is the Finger strain tensor, i.e., the inverse of the Cauchy–Green strain tensor  $C_t$ . The memory function  $m$  is written as:

$$m = \sum_i \frac{g_i \cdot f(\dot{\gamma}) \cdot \zeta(t, \dot{\gamma})}{\lambda_i} \cdot e^{(-\frac{t-t'}{\lambda_i})} \quad (2)$$

where  $\lambda_i$  and  $g_i$  are the relaxation times and relaxation modulus coefficients, respectively, at low shear rate or at rest;  $i$  is the number of relaxation spectra; and  $\dot{\gamma}$  is the shear rate. The strain-dependent function  $h$  used is the Papanastasiou–Scriven–Macosko (PSM) function [9,13–15].

The model contains four groups of parameters, i.e., the relaxation spectra, the parameter in the strain-dependent function, structural parameter  $f$  for considering the shear-rate effect, and structural parameter  $\zeta$  for considering both the shear-rate and shear-time effect simultaneously. All the parameters can be found in [9], where the relaxation spectra of the solution is obtained by fitting the frequency sweep experiment; the parameter in the strain-dependent function is obtained by fitting the stress relaxation experiment under step strain; parameter  $f$  is obtained according to the steady shear stress experiment; and parameter  $\zeta$  is from the start-up experiment, which is calculated using the linear interpolation method.

## 3. Results and Discussion

Based on the viscoelastic characterization of the micellar solution, the steady shear properties of the solution—such as the first normal stress difference ( $N_1$ )—were predicted in [9], which indicates some reasonable aspect of the viscoelastic theory studied here. As mentioned in the first part of the work [9], another five groups of transient shear experiments reported by Pipe et al. [3] can also be predicted to check the capability of the model. Below are the predictions.

### 3.1. Start-Up Experiment

Figures 8, 10 and 13, reported by Pipe et al. [3], present the stress growth in the step rate experiment (i.e., the start-up experiment) of the CPyCl/NaSal solution, and the differences among the three figures can be observed in the experimental data, where the shear stress growth in Figure 8 was employed to obtain parameter  $\zeta$ . The other three groups of experiments are predicted here.

#### 3.1.1. $N_1$

The growth of the first normal stress difference  $N_1$  in the step rate experiment is also shown in Figure 8, as reported in [3], which is shown here in Figure 1, along with the prediction using the Vasquez–Cook–McKinley (VCM) model and the calculated result from the modified RS-PSM model with both parameters,  $f$  and  $\zeta$ . The calculated results from both models show consistency with those from the experiments performed under the shear rate of  $5 \text{ s}^{-1}$ . At the shear rate of  $150 \text{ s}^{-1}$ , the result of the VCM model features a small and sharp stress-overshoot regime, which exhibits a large deviation from the experiment. The results of the present calculations at 30 and  $150 \text{ s}^{-1}$  also show deviations from the experimental data, but the results are improved appearance, indicating that both the present model and the parameters describing the viscoelastic properties of the CPyCl/NaSal solution in this study can reflect the  $N_1$  property of the solution more effectively. When the shear time reached 2 s and the stress had a steady status, the transient  $N_1$  in Figure 1 was equal to that calculated in the steady shear experiment in [9]. The reason for the inefficiency of the present model in predicting  $N_1$  is unknown. Remarkably, Gaudino et al. [16] predicted the transient  $N_1$  of the same CPyCl/NaSal solution with 50 mM of NaSal at least at a steady state using the parameters obtained in characterizing the shear stress growth data.

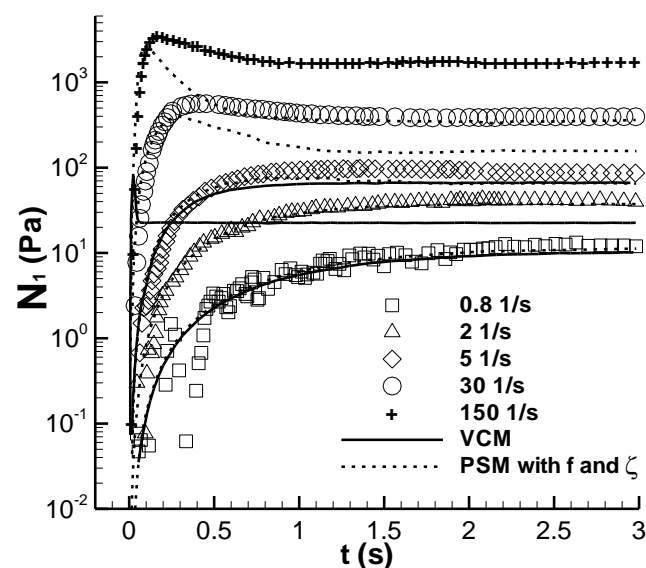


**Figure 1.** Transient  $N_1$  of the CPyCl/NaSal solution in the start-up experiment. Symbols are the experimental data in Figure 8 in the study conducted by Pipe et al. [3], and lines are the calculations. The calculated values for the VCM model are at 0.8, 5, and  $150 \text{ s}^{-1}$  [3], and “PSM with  $f$  and  $\zeta$ ” is the present calculation.

#### 3.1.2. Shear Stress

Figure 13, reported by Pipe et al. in [3], shows six groups of the experimental data in the step rate experiment, where three groups (the maximum shear stress in the stress growth after applying a step rate, the steady shear stress after long-term shear, and a group of stress growth data at the shear rate of  $70 \text{ s}^{-1}$ ) were obtained using a single step rate. The other three groups (the minimum shear stress at the second low shear rate, the steady shear stress after long-term shear, and a group of stress developing data at the shear rate of  $5 \text{ s}^{-1}$ )

after shearing at  $150 \text{ s}^{-1}$ ) were obtained using the two-step rates mode with a decreasing shear rate. Calculation of the two-step rates mode with a decreasing shear rate in this study was hindered by both the complex strain history and the deficiency of experimental data; therefore, the experiments involving the single-step rate were predicted.

Figure 2 shows the maximum shear stress in the step rate, including the experimental data denoted by ‘max’ and the calculations denoted by ‘max calculated’. The values calculated at  $1, 3, 10,$  and  $70 \text{ s}^{-1}$  are predictions, and those at  $5$  and  $30 \text{ s}^{-1}$  are fits. The maximum calculated value at  $70 \text{ s}^{-1}$  was approximately 33% lower than that obtained experimentally, which is attributed to the linear interpolation between the  $\zeta$  values at  $30$  and  $150 \text{ s}^{-1}$  and the large gap between those at the two shear rates.

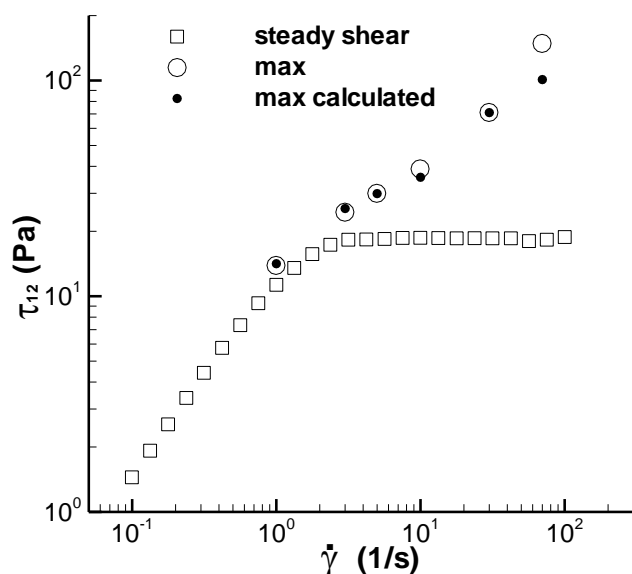


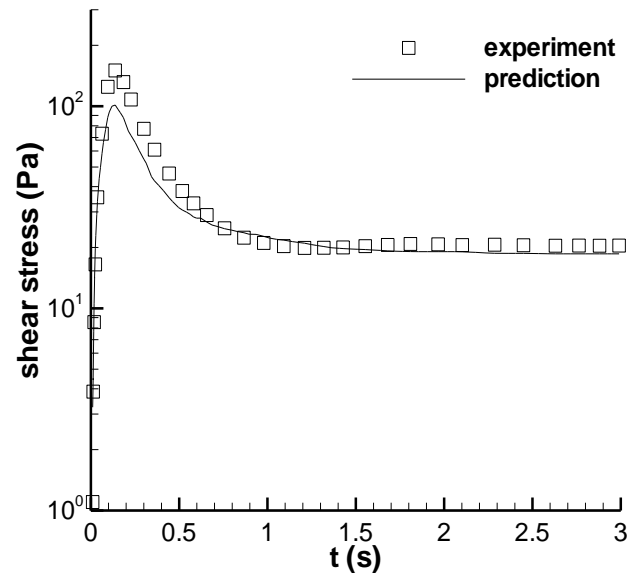
**Figure 2.** Maximum shear stress in step rate experiment and the steady shear stress of the CPyCl/NaSal solution. The square symbol is the steady experiment in Figure 6 of Pipe et al. [3], the circle is the transient experiment in Figure 13 of Pipe et al. [3], and the solid circle is the calculation here.

The prediction of the shear stress growth at the shear rate of  $70 \text{ s}^{-1}$  is shown in Figure 3. In the stress-overshoot regime, the calculation result is lower than the experimental result due to interpolation; however, in a different regime, the calculated result is consistent with the experiment result. From the  $\zeta$  curve in Figure 5 in the first part of the work [9], we can see that the  $\zeta$  values at both  $30$  and  $150 \text{ s}^{-1}$  in the overshoot regime are apparently larger than 1, which can cause corresponding calculation deviation at  $70 \text{ s}^{-1}$ , and those in the steady shear regime approach 1, which will produce a calculation result similar to the experiment.

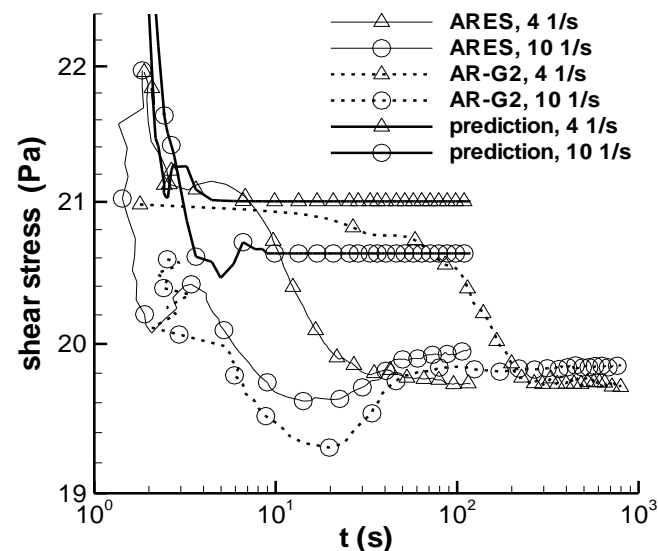
### 3.1.3. Long-Term Start-Up Experiment

Figure 10 in the study by Pipe et al. [3] presents a group of the experiments performed to show the difference between the step rate experiments obtained on two apparatuses, i.e., ARES and AR-G2 rheometer, and does not show the calculation of the VCM model. In this experiment group, the shearing time was long: 120 s for ARES and 800 s for AR-G2, and the shear rates were  $3, 4, 5,$  and  $10 \text{ s}^{-1}$ . The present modified RS-PSM model with parameters  $f$  and  $\zeta$  was employed to calculate the two experiments at  $4$  and  $10 \text{ s}^{-1}$ , shown in Figure 4. Under long-term shearing, the experimental stress exhibited a slightly decreasing trend and other subtle phenomena, and the calculated stress at  $4 \text{ s}^{-1}$  was  $21 \pm 0.5 \text{ Pa}$  after the shear time reached 2 s. For the calculation at  $10 \text{ s}^{-1}$ , reaching the steady state took slightly longer (approximately 2.5 s), and the stress was  $21 \pm 0.5 \text{ Pa}$ . The calculated stress was constant at approximately 10 s and did not exhibit subtle variation after 10 s, despite the slight

difference between the steady stresses at the two shear rates. The deviation between the calculated and experimental results was small, e.g., the deviation between the calculated steady stress and the minimum experimental shear stress was less than 7%. The maximum deviation in this case was approximately one-fifth of the deviation between the calculation result and the experiment result of the maximum overshoot stress in Figure 3.



**Figure 3.** Prediction of the stress growth at  $70 \text{ s}^{-1}$ . The symbol is the experiment in Figure 13 of Pipe et al. [3], and the line is the calculation here.



**Figure 4.** Long-term stress growth. Both the solid and the dashed lines are the experiments in Figure 10 of Pipe et al. [3], and the bold solid line is the calculation here.

### 3.2. Stress Relaxation Experiment

The stress relaxation experiment was conducted by first applying a step rate. Subsequently, the shear rate lasted a while until it reached a steady state for shear stress. Finally, the shearing was completed, but the recording of the shear stress variation over time was maintained. The stress in the sample upon cessation of the shearing decreased over time, and this phenomenon is called stress relaxation after steady shear. Pipe et al. [3] presented five groups of the stress relaxation experiments and three calculations of the VCM model at  $0.1, 2, \text{ and } 150 \text{ s}^{-1}$ . The present study also presents three calculations in the same conditions as those used by Pipe et al. [3], which are shown in Figure 5. The predictions of the present

model are similar to those of the VCM model at the three shear rates; however, certain deviations can be observed between the experimental and calculated results. Pipe et al. [3] also used a two-mode exponential relaxation process to adequately describe the relaxation experiment at  $150 \text{ s}^{-1}$ ; however, the structuralized model in the present study was not modified using this method to improve the calculation results.

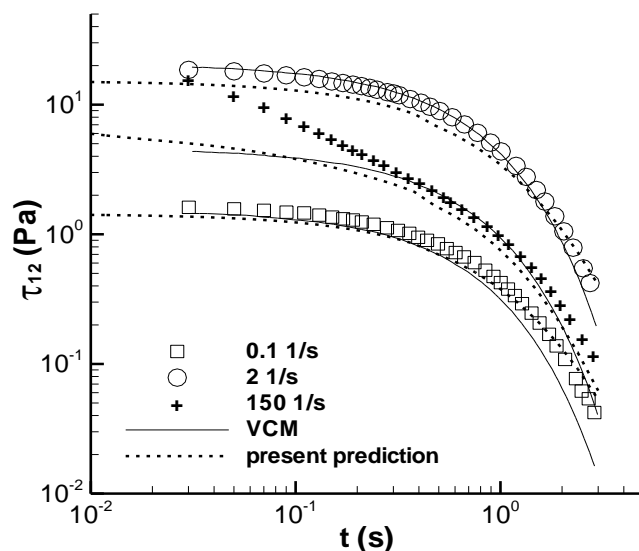


**Figure 5.** Stress relaxation property of the CPyCl/NaSal solution after steady shear. The symbols represent the experimental data in Figure 9 reported by Pipe et al. [3], and lines represent the calculated results. The solid line is the prediction of Pipe et al. [3], and the dashed line is the present calculation.

### 3.3. Step Strain Experiment

In the study by Pipe et al. [3], Figure 5 shows two groups of experimental data, i.e., the relation between  $N_1/\tau_{12}$  and time  $t$  and the relation between  $N_1/\tau_{12}$  and strain  $\gamma$  in the step strain experiment, as well as the prediction of the VCM model. According to the calculation process of the VCM model [3], the strain history of the step strain experiment can be formed by applying a triangular-like shear rate, such that the strain increases and reaches a constant at the end of shearing. Therefore, the strain application process in the calculation is indeed an applying-rate process, where the shear rate is applied according to a designed rule. The complex application of the shear rate used in the study by Pipe et al. [3] was not possible in this study, and the step rate mode was used to generate a strain on the sample. This is why the step rate was added to the experimental mode of this group of experiment in Table 1 [9].

**Table 1.** Three modes of applying the shear rate.

$\gamma$	Mode 1		Mode 2		Mode 3	
	$\dot{\gamma} \text{ (s}^{-1}\text{)}$	$t_0 \text{ (s)}$	$\dot{\gamma} \text{ (s}^{-1}\text{)}$	$t_0 \text{ (s)}$	$\dot{\gamma} \text{ (s}^{-1}\text{)}$	$t_0 \text{ (s)}$
1	150	0.006667	10	0.1	16.67	0.06
2		0.01333	20		33.33	0.06
4		0.02667	40		61.54	0.065
6		0.04000	60		75	0.08
8		0.05333	80		100	0.08
10		0.06667	100		125	0.08
12		0.08000	120		133.3	0.09

Three modes of shear rate application were employed here to generate the seven strains used in the step strain experiment conducted by Pipe et al. [3]. The first application

of the shear rate of  $150 \text{ s}^{-1}$  was denoted by “Mode 1”, and the shear time used was calculated using the given strain. The shear time  $t_0$  in Table 1 is obviously long as the strain is large. In terms of the  $N_1/\tau_{12}$  versus  $t$  experiment in Figure 5 reported by Pipe et al. [3], the shear stress approached a steady state or the maximum level at approximately 0.1 s. Therefore, the second mode, denoted by “Mode 2”, involves the use of 0.1 s as the shear time. Therefore, the shear rate can be calculated by dividing the strain by the shear time. Finally, the shear time of 0.1 s is adjusted manually and slightly according to the calculations of Mode 2 and the  $N_1/\tau_{12}$  experiments, which is denoted by “Mode 3” in Table 1.

Figure 6 shows the calculated  $N_1/\tau_{12}$  versus  $t$  relation in the CPyCl/NaSal solution using the three shear rate modes in Table 1 and the experimental and calculated  $N_1/\tau_{12}$  versus  $\gamma$  relation. The steady  $N_1/\tau_{12}$  values of the three shear rate modes are almost identical and almost correspond to the experimental data in Figure 6a. The difference between the calculations of the three modes is the time taken to reach a steady state of  $N_1/\tau_{12}$ , which is equal to the shear time  $t_0$ . The overshoot of  $N_1/\tau_{12}$  is also not observed in the calculation, and the  $N_1/\tau_{12}$  calculated is almost constant after  $t_0$ . However, the experimental  $N_1/\tau_{12}$  exhibits an overshoot phenomenon at large strain and approaches a constant after 0.1 s, but it is not stable. Figure 6b shows the results of the VCM model, where the curve of the VCM model at  $\gamma = 1$  is consistent with the experiment after 0.1 s, and the other two curves at  $\gamma = 6$  and  $\gamma = 12$ , respectively, show large deviations from the corresponding experiments. The results of Mode 3 are consistent with those of the experiments, including both the steady  $N_1/\tau_{12}$  value and the time reaching the steady state or the maximum stress ratio. The consistency of time between the experiment and the calculation is attributed to the artificial adjustment of shear time according to the experiment; however, this consistency also reflects the capability of the present modified RS-PSM model with parameters  $f$  and  $\zeta$  to fairly express the viscoelastic property of the micellar solution.

Figure 6c shows a clear deviation between the results of the experiment and the calculation of the VCM model, and the experimental data are consistent with the Lodge–Meissner relation, i.e.,  $N_1/\tau_{12} = \gamma$ , under the strain of 9, which indicates some deficiency of the VCM model. The present calculation using Mode 3 approaches both the experiment and the Lodge–Meissner relation, which shows a certain reasonable aspect of the present model. In the analysis of the data on  $N_1/\tau_{12}$  versus  $\gamma$ , Pipe et al. [3] proposed that the deviation between the calculation of the VCM model and the experimental result could be related to the inhomogeneous flow of the solution, and the present calculation shows another possible explanation of such a viscoelastic phenomenon, i.e., the homogeneous flow could produce more of the experimental phenomena of  $N_1/\tau_{12}$  versus  $\gamma$  curve owing to the viscoelastic property of the solution. In addition, the influence of applying the real shear strain in the calculation remains unknown, despite the attempted application of three modes, because all three modes differ from the experimental process used by Pipe et al. [3]. This could complicate the present calculation.

Theoretical analysis on the viscoelastic property of micellar solution is an attractive topic, and at least seven such papers have been composed in 2022 [9,17–22]. The work of Pipe et al. [3] was cited in refs. [9,17,19–21], in which ref. [9]—i.e., the first part of the present work—showed a detailed characterization on the viscoelasticity of the micellar solution of the authors, albeit using a different method. The authors of the other four papers [19,19–21] only introduced the work of Pipe et al. [3] without analyzing the experimental data, using the viscoelastic theoretical model. Therefore, the present predictions on the viscoelastic properties of the micellar solution of Pipe et al. can promote the understanding on the abundant experimental viscoelastic behaviors of the micellar solution; moreover, they can further show the capability of the adopted model, although the viscoelastic behaviors of the solution still cannot be fully described by it.

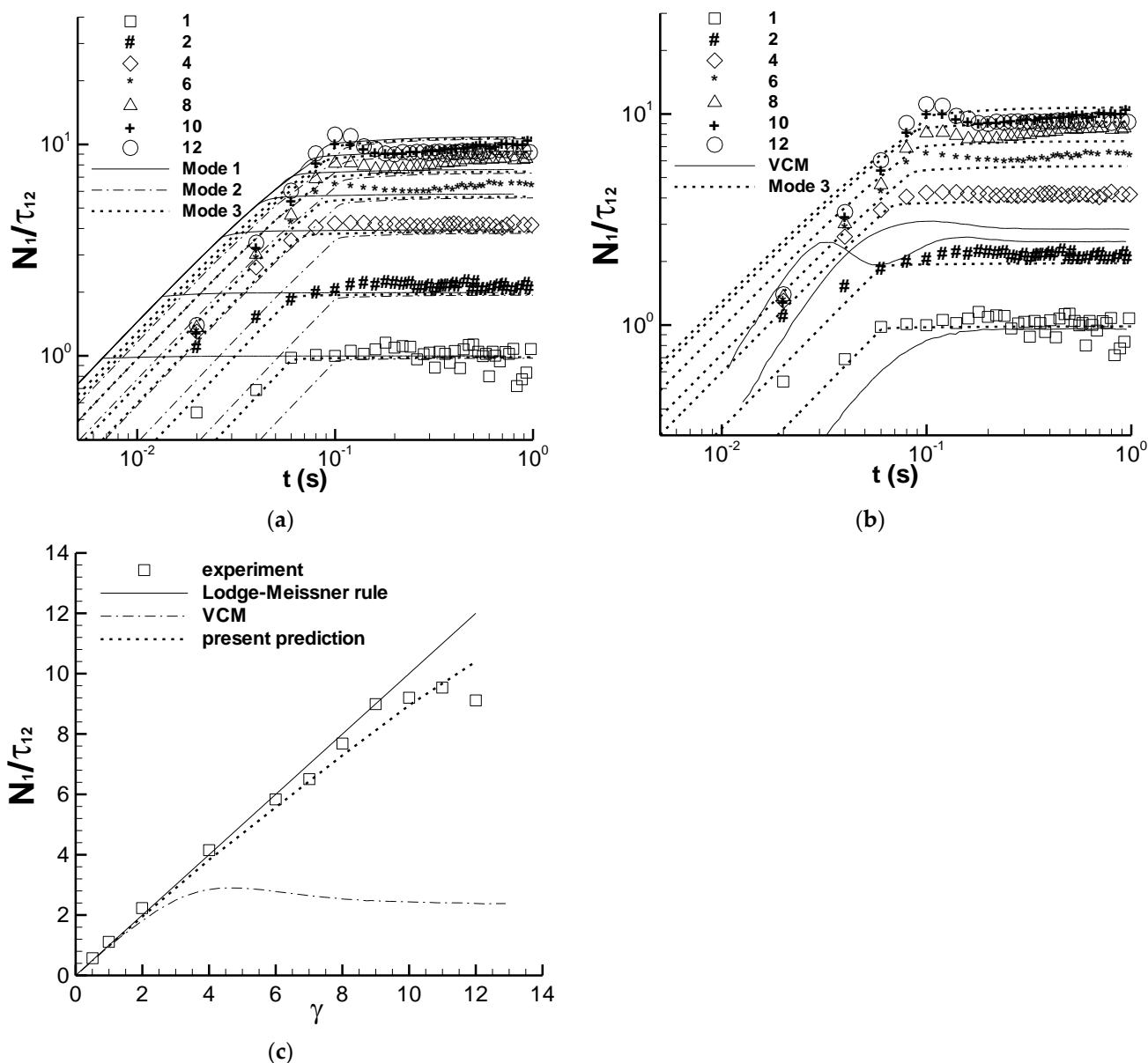


**Figure 6.** (a) Relation of  $N_1/\tau_{12}$  versus  $t$  obtained using three shear rate modes, (b)  $N_1/\tau_{12}$  of both Mode 3 and VCM model, (c) the correlation between  $N_1/\tau_{12}$  and  $\gamma$ . The symbols represent the experimental data in Figure 5 of Pipe et al. [3], and the lines are calculations, in which “VCM” and “Lodge-Meissner rule” are from Pipe et al. [3], and “Mode 1”, “Mode 2”, “Mode 3”, and “present prediction” are the present calculations.

#### 4. Conclusions

The theoretical characterization on the viscoelastic properties of the CPyCl/NaSal wormlike micellar solution at 22 °C was employed in this study to predict five groups of transient shear viscoelastic behaviors of the solution, which are summarized here.

(1) The prediction of the transient  $N_1$  in the stress growth experiment was improved.

(2) The structuralized model in this study yielded reasonable results with respect to the maximum shear stress in the start-up experiment. The stress growth calculated at  $70 \text{ s}^{-1}$  was low for the maximum shear stress in the stress-overshoot regime owing to the deficiencies of both  $\zeta$  data and the linear interpolation method. During the long-term shearing in the start-up experiment, the model yielded a steady state value, and the experiment showed a slight decrease or variation, but the deviation between the steady calculated stress and the minimum experimental stress was less than 7%.

(3) The present calculation results are similar to those of the VCM model on the stress relaxation upon cessation of steady shear flow.

(4) Both the experiment of  $N_1/\tau_{12}$  versus  $\gamma$  and the Lodge–Meissner relation under the strain of 9 in step strain can be adequately expressed by the model.

In summary, the prediction capability of the present model with respect to the stress relaxation experiment approached that of the VCM model, and the other four groups of predictions were clearly improved (see Figures 1 and 6) or firstly shown (see Figures 2–4). For example, the experimental  $N_1/\tau_{12}$  was 9 at the strain of 9 in the step strain experiment in Figure 6c, and the corresponding previous and present predictions were 2.47 and 8.45, respectively. These results indicate that the model and parameters in the present study are relatively more suitable for describing the viscoelastic properties of the CPyCl/NaSal solution at 22 °C.

In Figure 7 of the paper published by Pipe et al. [3], the second normal stress difference coefficient, which was neither used nor predicted in the present study, is shown. The method for including the effect of the second normal stress difference  $N_2$  in the RS equation [14,23] was not included in the present model; therefore, the  $N_2$  experiment was not used. Moreover, another group of data—i.e., Figures 11 and 12 reported by Pipe et al. [3]—that were obtained by applying designed stress were not predicted. In the present model, stress is a function of deformation or shear rate; therefore, the model cannot be used to calculate the shear rate by inputting the shear stress. The step stress experiment should be calculated in future studies.

**Funding:** This research was partly funded by the Foundation of Shanghai Jiao University, grant number JG010003/006.

**Institutional Review Board Statement:** Not applicable.

**Data Availability Statement:** The data that support the findings of this study are available within the article.

**Conflicts of Interest:** The author declares no conflict of interest.

## References

1. Arjmand, O.; Roostaei, A. Experimental investigation of viscous surfactant based enhanced oil recovery. *Pet. Sci. Technol.* **2014**, *32*, 1607–1616. [[CrossRef](#)]
2. Jeirani, Z.; Mohamed Jan, B.; Si Ali, B.; See, C.H.; Saphanuchart, W. Pre-prepared microemulsion flooding in enhanced oil recovery: A review. *Pet. Sci. Technol.* **2014**, *32*, 180–193. [[CrossRef](#)]
3. Pipe, C.J.; Kim, N.J.; Vasquez, P.A.; Cook, L.P.; McKinley, G.H. Wormlike micellar solutions. II: Comparison between experimental data and scission model predictions. *J. Rheol.* **2010**, *54*, 881–914. [[CrossRef](#)]
4. Zhao, Y.; Haward, S.J.; Shen, A.Q. Rheological characterizations of wormlike micellar solutions containing cationic surfactant and anionic hydrotropic salt. *J. Rheol.* **2015**, *59*, 1229–1259. [[CrossRef](#)]
5. Ahmadi, M.A.; Shadizadeh, S.R.; Salari, Z. Dependency of critical micellization concentration of an anionic surfactant on temperature and potassium chloride salt. *Pet. Sci. Technol.* **2014**, *32*, 1913–1920. [[CrossRef](#)]
6. Ahmadi, M.; Ahmad, Z.; Phung, L.T.K.; Kashiwao, T.; Bahadori, A. Experimental investigation the effect of nanoparticles on micellization behavior of a surfactant: Application to EOR. *Pet. Sci. Technol.* **2016**, *34*, 1055–1061. [[CrossRef](#)]
7. Kumar Sinha, A.; Bera, A.; Raipuria, V.; Kumar, A.; Mandal, A.; Kumar, T. Numerical simulation of enhanced oil recovery by alkali-surfactant-polymer floodings. *Pet. Sci. Technol.* **2015**, *33*, 1229–1237. [[CrossRef](#)]
8. Pannu, S.; Phukan, R.; Tiwari, P. Experimental and simulation study of surfactant flooding using a combined surfactant system for enhanced oil recovery. *Pet. Sci. Technol.* **2022**, *40*, 2907–2924. [[CrossRef](#)]
9. Huang, S. Prediction of the viscoelastic properties of a cetyl pyridinium chloride/sodium salicylate micellar solution: (I) characterization. *Pet. Sci. Technol.* **2022**. [[CrossRef](#)]
10. Huang, S. Structural viscoelasticity of a water-soluble polysaccharide extract. *Int. J. Biol. Macromol.* **2018**, *120*, 1601–1609, Erratum in *Int. J. Biol. Macromol.* **2021**, *193*, 2389. [[CrossRef](#)]
11. Huang, S. Viscoelastic characterization and prediction of a wormlike micellar solution. *Acta Mech. Sin.* **2021**, *37*, 1648–1658, Erratum in *Acta Mech. Sin.* **2021**, *37*, 1714. [[CrossRef](#)]
12. Huang, S. Viscoelastic property of an LDPE melt in triangular- and trapezoidal-loop shear experiment. *Polymers* **2021**, *13*, 3997. [[CrossRef](#)] [[PubMed](#)]
13. Papanastasiou, A.C.; Scriven, L.E.; Macosko, C.W. An integral constitutive equation for mixed flows: Viscoelastic characterization. *J. Rheol.* **1983**, *27*, 387–410. [[CrossRef](#)]

14. Bird, R.B.; Armstrong, R.C.; Hassager, O. *Dynamics of Polymeric Fluids, Vol. 1. Fluid Mechanics*, 2nd ed.; Wiley: New York, NY, USA, 1987.
15. Laun, H.M.; Schmidt, G. Rheotens tests and viscoelastic simulations related to high-speed spinning of Polyamide 6. *J. Non-Newton. Fluid Mech.* **2015**, *222*, 45–55. [[CrossRef](#)]
16. Gaudino, D.; Costanzo, S.; Ianniruberto, G.; Grizzuti, N.; Pasquino, R. Linear wormlike micelles behave similarly to entangled linear polymers in fast shear flows. *J. Rheol.* **2020**, *64*, 879–888. [[CrossRef](#)]
17. Sato, T.; Larson, R.G. Nonlinear rheology of entangled wormlike micellar solutions predicted by a micelle-slip-spring model. *J. Rheol.* **2022**, *66*, 639–656. [[CrossRef](#)]
18. Tan, G.; Larson, R.G. Quantitative modeling of threadlike micellar solution rheology. *Rheol. Acta* **2022**, *61*, 443–457. [[CrossRef](#)]
19. Hopkins, C.C.; Haward, S.J.; Shen, A.Q. Upstream wall vortices in viscoelastic flow past a cylinder. *Soft Matter* **2022**, *18*, 4868–4880. [[CrossRef](#)]
20. Varchanis, S.; Haward, S.J.; Hopkins, C.C.; Tsamopoulos, J.; Shen, A.Q. Evaluation of constitutive models for shear-banding wormlike micellar solutions in simple and complex flows. *J. Non-Newton. Fluid Mech.* **2022**, *307*, 104855. [[CrossRef](#)]
21. López-Aguilar, J.E.; Resendiz-Tolentino, O.; Tamaddon-Jahromi, H.R.; Ellero, M.; Manero, O. Flow past a sphere: Numerical predictions of thixo-viscoelastoplastic wormlike micellar solutions. *J. Non-Newton. Fluid Mech.* **2022**, *309*, 104902. [[CrossRef](#)]
22. Patel, M.C.; Ayoub, M.A.; Hassan, A.M.; Idress, M.B. A novel ZnO nanoparticles enhanced surfactant based viscoelastic fluid systems for fracturing under high temperature and high shear rate conditions: Synthesis, rheometric analysis, and fluid model derivation. *Polymers* **2022**, *14*, 4023. [[CrossRef](#)] [[PubMed](#)]
23. Luo, X.L.; Tanner, R.I. Finite element simulation of long and short circular die extrusion experiments using integral models. *Int. J. Numer. Meth. Eng.* **1988**, *25*, 9–22. [[CrossRef](#)]